

## Article

# Near Infrared Illumination Optimization for Vein Detection: Hardware and Software Approaches

Abu Bakar Abd Rahman <sup>1</sup>, Floressy Juhim <sup>1</sup>, Fuei Pien Chee <sup>1,\*</sup>, Abdullah Bade <sup>2</sup> and Fairrul Kadir <sup>3</sup>

<sup>1</sup> Faculty of Science and Natural Resources (FSNR), Universiti Malaysia Sabah, Kota Kinabalu 88400, Sabah, Malaysia

<sup>2</sup> Mathematics, Graphics and Visualization Research Group (M-GRAVS), Universiti Malaysia Sabah, Kota Kinabalu 88400, Sabah, Malaysia

<sup>3</sup> Faculty of Medicine and Health Science, Universiti Malaysia Sabah, Kota Kinabalu 88400, Sabah, Malaysia

\* Correspondence: fpchee06@ums.edu.my

**Abstract:** Venepuncture is one of the most crucial processes in many medical procedures. However, finding a real-time and vibrant visualization of the vein structures faces many difficulties. Several devices were introduced to solve this problem, yet, these devices shared common drawbacks, primarily when visualizing deep veins or veins in a thicker tissue of the human body. This study proposes a novel method for visualizing vein structures using a near-infrared (NIR) imaging technique enhanced with Hessian ridge detection. Several factors, including the wavelength of NIR light, square LED and ring LED arrangement and the effect of the diffuser and number of LEDs, were evaluated in the study. This study improves the overall quality of the acquired vein images and highlights the vein-morphological structure through image processing techniques. The study's main aim is to achieve the highest number of visible veins. Based on the optical window, the maximum absorption range in the NIR spectrum was found from 700 to 950 nm. The NIR light absorption of human deoxygenated blood in the vein was highest at 850 nm peak of wavelength. The image processing further enhances the vein image by highlighting the extracted vein. The study also suggests that the square LED arrangements of NIR illumination are much more robust than the ring LED arrangement in ensuring excellent light penetration. The light diffuser further adds promising effects to the NIR illumination process. In terms of the square LED arrangement, increasing the square LED for enlarging the illumination area did not show any degradation effects in the visualization process. Overall, this paper presents an integrated hardware and software solution for the NIR image acquisition of a vein visualization system to cope with the image visualization of the vein for a thicker part of the human tissue, particularly on the arm and palm area.

**Keywords:** infrared imaging; near infrared; vein detection; NIR projection; infrared LEDs wavelength; LEDs arrangement; vein counting



**Citation:** Abd Rahman, A.B.; Juhim, F.; Chee, F.P.; Bade, A.; Kadir, F. Near Infrared Illumination Optimization for Vein Detection: Hardware and Software Approaches. *Appl. Sci.* **2022**, *12*, 11173. <https://doi.org/10.3390/app12211173>

Academic Editors: Vladislav Toronov and Mario Gai

Received: 6 September 2022

Accepted: 25 October 2022

Published: 4 November 2022

**Publisher's Note:** MDPI stays neutral with regard to jurisdictional claims in published maps and institutional affiliations.



**Copyright:** © 2022 by the authors. Licensee MDPI, Basel, Switzerland. This article is an open access article distributed under the terms and conditions of the Creative Commons Attribution (CC BY) license (<https://creativecommons.org/licenses/by/4.0/>).

## 1. Introduction

NIR imaging is one of the emerging technologies to facilitate vein detection. It is especially beneficial for the peripheral IV catheter to gain access to a vein. Although the reviewed devices had demonstrated usefulness for peripheral veins visualization, the other evaluated factors were less definite to preclude any general conclusions about their overall performance. The utilization of NIR technology is a novel technique and started to receive research interest since 2010. However, the availability of these commercial devices related to image acquisition techniques remained an unsolved issue due to the deficiency of the performance and the high costs of the devices. Thus, it is crucial to study the essential parameters for enhancing the image acquisition approach to obtain a higher-quality vein image. This paper presents the proposed enhancement of the vein visualizing system. Four essential parameters were investigated: evaluation of NIR peak wavelength, LEDs arrangement for light illumination

purposes, the effect of the diffuser and the number of illumination LEDs. This research also focuses on developing a highly affordable, integrated, portable vein visualization device that uses low-cost commercial off-the-shelf electronic components.

Venepuncture and intravenous cannulation are among the most common medical procedures that were performed on patients [1]. In a human blood vessel, it contains information for health monitoring and possible diseases that can be detected [2]. However, finding a good visualization of vein structures [3] is often difficult. Thus, the nurse has no choice but to perform based on their anatomical knowledge and experience [3]. This sometimes leads to some errors, which may cause direct or indirect harm to the patient.

Infrared radiation is a good preference since it can penetrate up to several centimeters into tissues [1]. The maximum absorption range was found in the near-infrared spectrum (700–900 nm) for NIR-I, as discussed by Azueto-rios, 2016 [4]. While Crisan and Tebrean, 2017, revealed that near-infrared radiation (NIR) is strongly absorbed by both veins and arteries using a narrow radiation window of 750–950 nm, water has a reduced influence on the scanning. Veins strongly absorb NIR radiation based on a narrow optical window. Different wavelengths show different behavior of haemoglobin together with water when illuminated with NIR radiation. Therefore, the optical window can be chosen between 700 and 950 nm. Infrared radiation is absorbed by haemoglobin in the blood vessels while the surrounding tissues other than the blood vessels do not absorb infrared radiation but reflect it [5]. When capturing an image of the blood vessels, it will appear darker than the other parts as they absorb infrared light [2]. Infrared radiation is capable of capturing the superficial vein inside the human body [6].

Nundy and Sanyal, 2010, discussed a vein pattern extraction algorithm for biometric identification. Using low-quality sensors, they studied image acquisition and pattern detection techniques for veins and proposed a technique to detect tissue patterns using thermal (IR) imaging. However, the research is much more complicated and requires costly equipment. There is another type of device that uses far-infrared (FIR) light, where a thermal camera is used to obtain images of procedures ranging from visualizing vein structures to performing segmentation; however, it still encounters the disadvantage of high-cost equipment [3]. Other vein visualization devices use penetration methods of NIR light. Nonetheless, current devices have drawbacks, whereby they are big and inconvenient to use during venepuncture [3]. In the latest studies, a vein camera mobile application to obtain NIR images was designed by Print and Qadir, 2019 [7]. This was followed by the design of a low-cost system to detect the veins in the palm by Alwazzan, 2020 [8]. Further quantitative and experimental studies are needed to achieve the optimal results of the vein image. There has also been substantial work in designing mobile devices with biomedical and biometric capabilities.

Although various vein viewer devices are commercially available, the high cost has become the bottleneck for making the assisted devices used extensively by medical practitioners in hospitals and clinics. Most commercial vein viewers were developed by using complex systems with the integration of laser scanning mechanisms making the cost for fabrication of such devices higher. Hence, the alternative solution is to utilize low-cost near-infrared vein medical imaging. To date, various approaches in hardware and software by the utilization of low-cost commercial off-the-shelf electronic sensors are still progressing [9,10].

## 2. Methodology

The flowchart of the overall study is shown in Figure 1. The methodologies were carried out to achieve the objectives of this study.

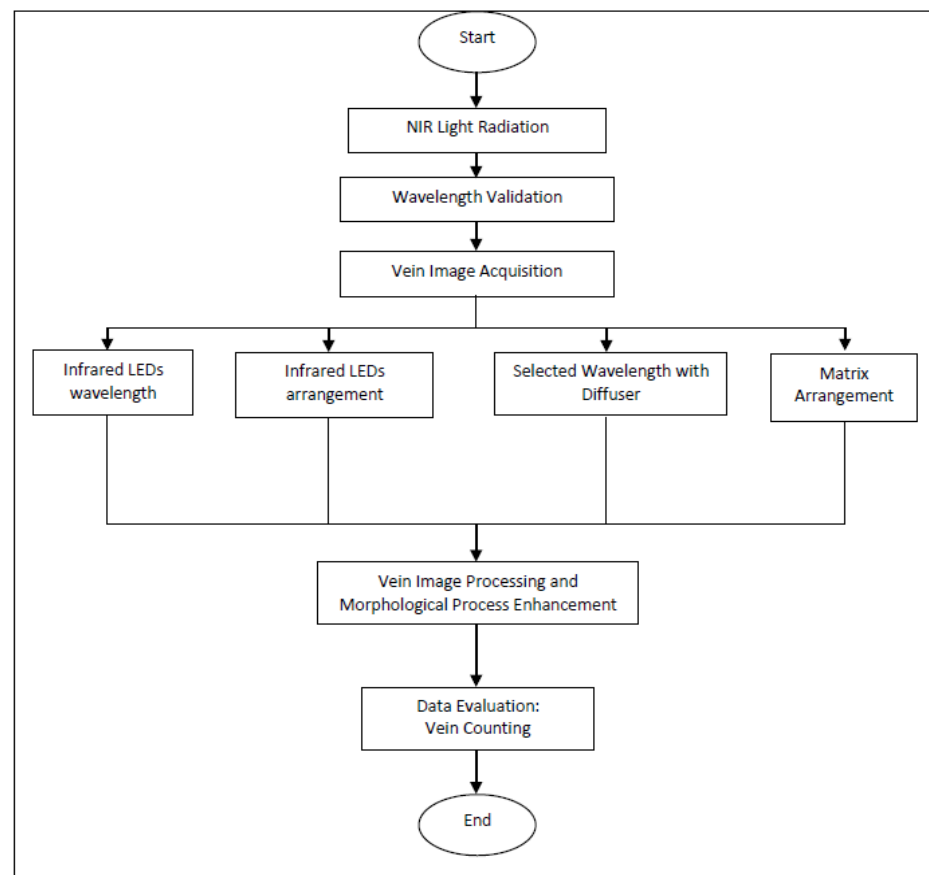


**Figure 1.** Flowchart of Overall Study.

### 2.1. NIR Projection

Different LEDs configurations were tested to compare their visualization performance depending on the parameter settings, which include LED wavelength, luminosity, and angle of illumination.

#### 2.1.1. LED Wavelength

Five near-infrared LEDs with different peak wavelengths (720 nm, 760 nm, 850 nm, 900 nm, and 940 nm) were tested in terms of absorption on the vein. The infrared-based sampling mainly utilizes the properties of infrared rays and infrared emission [11]. The wavelength being studied is in the range of near-infrared radiation based on the absorption in human blood. Excellent veins visualization can only be achieved by illuminating the skin with an incident of infrared light radiation of a specific wavelength. Otherwise, the incident light cannot penetrate the skin to reach the deeper veins and could not be reflected. Therefore, in an illumination approach, among the crucial factors of a vein visualization system is wavelength selection. An evaluation of different light sources with a selected range of 700 nm to 1000 nm wavelengths as suggested by Swarbrick and Boylan was carried out to assess the best reflection of the vein in the detection process [12].

#### 2.1.2. Luminosity

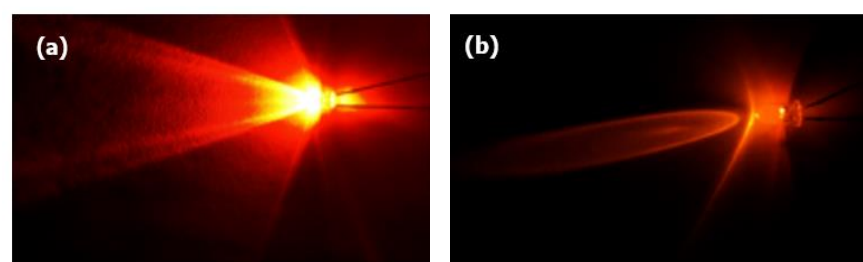
The NIR LEDs need to have a significant luminous intensity to achieve a homogeneous illumination in the field of view (FOV) of the acquisition system. The FOV must be properly illuminated. Hence, a larger FOV will require higher luminous intensity. Without uniform illumination, the vessels will not be recognized accurately. Therefore, luminosity is an important parameter in a transillumination veins visualization system. In this study, the specification of the NIR LEDs is shown in Table 1.

**Table 1.** Specifications of LEDs.

Wavelength	Specifications	Value
720 nm	DC Forward Current	20 mA
	Power Dissipation	150 mW
	DC Forward Voltage	1.6–2.0 V
	Luminous Intensity	5.46–9.56 cd
760 nm	DC Forward Current	20 mA
	Power Dissipation	150 mW
	DC Forward Voltage	1.6–2.0 V
	Luminous Intensity	6.83–10.93 cd
850 nm	DC Forward Current	200 mA
	Power Dissipation	180 mW
	DC Forward Voltage	1.8–2.3 V
	Luminous Intensity	30.74–92.21 cd
900 nm	DC Forward Current	100 mA
	Power Dissipation	40 mW
	DC Forward Voltage	2.2 V
	Luminous Intensity	6.83–10.93 cd
940 nm	DC Forward Current	100 mA
	Power Dissipation	150 mW
	DC Forward Voltage	1.4–1.8 V
	Luminous Intensity	40.98–58.06 cd

### 2.1.3. Angle

The incident light source angle also plays a crucial role in ensuring uniform illumination. LEDs with a very small angle of  $<15^\circ$  will illuminate isolated areas in a spot way, creating black holes in the center of the FOV which leads to difficulties in the visualization process. On the other hand, very wide angles make the light difficult to focus. Hence, choosing a proper angle for the illumination process is essential. LEDs with an illumination angle of  $>30^\circ$  were found to be a good angle for the LEDs parameter in line with Garcia and Horche finding as illustrated in Figure 2 [13]. Based on Table 2, LEDs with an illumination angle of  $30^\circ$  were utilized in this study.

**Figure 2.** LEDs with an angle of illumination at (a)  $30^\circ$  (b)  $15^\circ$ .**Table 2.** Angle of illumination of LEDs.

Wavelength	Angle
720 nm	$30^\circ$
760 nm	$30^\circ$
850 nm	$30^\circ$
900 nm	$30^\circ$
940 nm	$30^\circ$

The incident light wavelength emitted by the infrared LEDs was first examined using the ASEQ LR1 spectrometer. The absorption spectra were measured with the ASEQ

LR1 spectrometer (200–1200 nm, 2 nm resolution with 50  $\mu\text{m}$  slit) featuring a Toshiba TCD1304DG linear array (3648 pixels). The spectrometer was coupled with the ASEQ light source and ASEQ fiber-optics probe consisting of two fibers, one for excitation and one for collection. The fiber optic connector is SMA 905 to 0.22 numerical aperture with single-strand optical fiber. The absorption spectra of the LEDs were acquired with the ASEQ LR1 system.

The ASEQ LR1 spectrometer software was utilized to plot the wavelength captured by the instrument to verify the actual light wavelength output as emitted by the LEDs. Before the wavelength readings were taken, the instrument was first calibrated prior to this study to remove the noise from the surrounding light. Figure 3 shows the measured actual wavelength spectra of the selected NIR. Referring to Figure 3, the wavelength validation for (a) 720 nm, (b) 760 nm, (c) 850 nm, (d) 900 nm, and (e) 940 nm showed the wavelength emitted by the selected LEDs has a correct range of peak value.

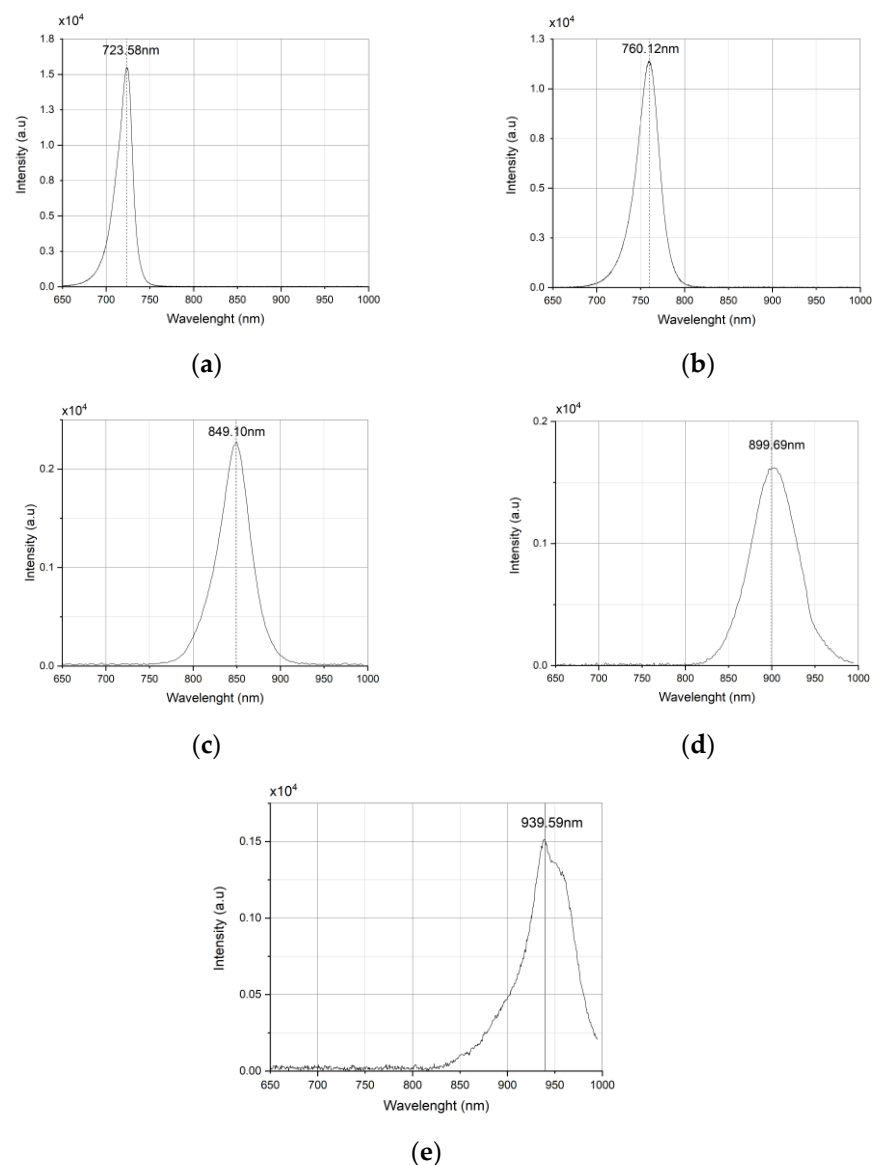


**Figure 3.** The wavelength spectra for LED wavelength of: (a) 740 nm; (b) 760 nm; (c) 850 nm; (d) 900 nm; and (e) 940 nm.

## 2.2. Vein Image Acquisition

### 2.2.1. Experiment Setup

The single-board computer Raspberry Pi 3 was used to process and store the captured image. The regions of interest (ROI) in this research were the palm and arm areas. The distance between cameras was kept constant at 15cm as it provides an ideal resolution [14] in the ROI and image acquisition, the experimental setup is shown in Figure 4. The ROI was illuminated with the NIR light at different wavelengths (720 nm, 760 nm, 850 nm, 900 nm, and 940 nm), two different LEDs arrangements (Square LED, Ring LED) and different square LED arrangements ( $3 \times 3$ ,  $4 \times 4$ ,  $5 \times 5$ ,  $6 \times 6$ ). The purpose of increasing the square LED arrangement and the diffuser on the light illuminations is to achieve optimal diffusing potential and gives the best result for vein viewing [15]. Figure 5 shows the configuration of the ring LED and square LED arrangement. The infrared source and camera were placed side by side to ensure a good match lighting system in the ROI area. The infrared LEDs were powered by a power source of 9 V. The lighting from the environment was kept constant with an average luminous emittance of 27.1 cd.

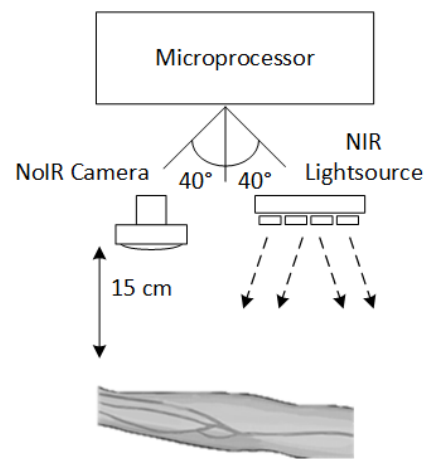


**Figure 4.** The experimental setup of the equipment.

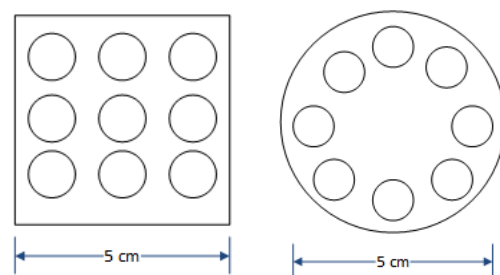


**Figure 5.** The LEDs arrangement for square LED (left) and ring LED (right).

The Pi NoIR was paired with a Raspberry Pi 3 to capture the raw images. The Raspberry Pi Foundation, the developers of an affordable but competent System on a Chip microcomputer, produced the PI NoIR, a 5 MP camera with a complete manual [16]. The Pi NoIR camera does not have an infrared filter, increasing the sensitivity to capture infrared images. Figure 6 shows the PI NoIR camera.

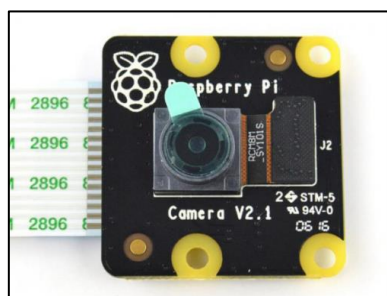


Figure 6. The Pi NoIR camera.

### 2.2.2. Design Parameters

Several design parameters were investigated to determine the optimum illumination source and structural factors in vein detection systems that optimize the visualization. The critical parameters must be fine-tuned to improve the visualization process of the vein to achieve the highest image quality. The parameters of interest are: (i) wavelength, (ii) LEDs arrangement, (iii) presence of diffuser, and (iv) square LED light source arrangement. Other parameters that are set to be constant in this experimental setup are average luminance intensity, exposure time, and distance of the light source. The experimental code name was assigned according to the following criteria:

- Method: Hessian (H), Contrast (C)
- Region of Interest (ROI): Palm (P), Arm (A)
- Wavelength: 720 nm (72), 760 nm (76), 850 nm (85), 900 nm (90), 940 nm (94)
- LEDs Arrangement: Square LED (M), Ring LED (R)
- Square LED Arrangement: 3 × 3, 4 × 4, 5 × 5, 6 × 6
- Number of LEDs: 8, 9, 16, 25, 36
- The inclusion of diffuser: Without diffuser (WO), With diffuser (W)

Table 3 below presents some of the code-name for the sample image obtained:

Table 3. Code-name for naming obtained sample image.

HP85M16WO					
H	P	85	M	16	WO
Method (Hessian)	ROI (Palm)	Wavelength (850 nm)	LEDs Arrangement (Square LED)	Number of LEDs (16)	Inclusion of Diffuser (No)
CA85R8					
C	A	85	R	8	
Method (Contrast)	ROI (Arm)	Wavelength (850 nm)	LEDs Arrangement (Ring LED)	Number of LEDs (8)	
CP85M3X3					
C	P	85	M	3X3	
Method (Contrast)	ROI (Palm)	Wavelength (850 nm)	LEDs Arrangement (Square LED)	Square LED arrangement	

### 2.3. Vein Image Processing and Morphological Process Enhancement

Several image processing approaches were implemented to ensure the captured vein image appears to be highly visible. Figure 7 illustrates the flowchart of the image processing system. The enhancement procedures started by first segmenting the vein image into the desired regions of interest (ROI). Then, it was followed by enhancing the quality of the vein image so that the procedure of extracting the ridge’s features was achievable. All image processing procedures were written in Python3 script and OpenCV libraries to facilitate the whole enhancement process. The resolution of the vein image was resized to 572 × 432 pixels for the image processing and enhancement process. The preferred image

resolution follows the near-infrared device and has a remarkable reduction percentage in the computational running time process. Figure 7 illustrates the overall image and morphological enhancement processing to produce the intended output.

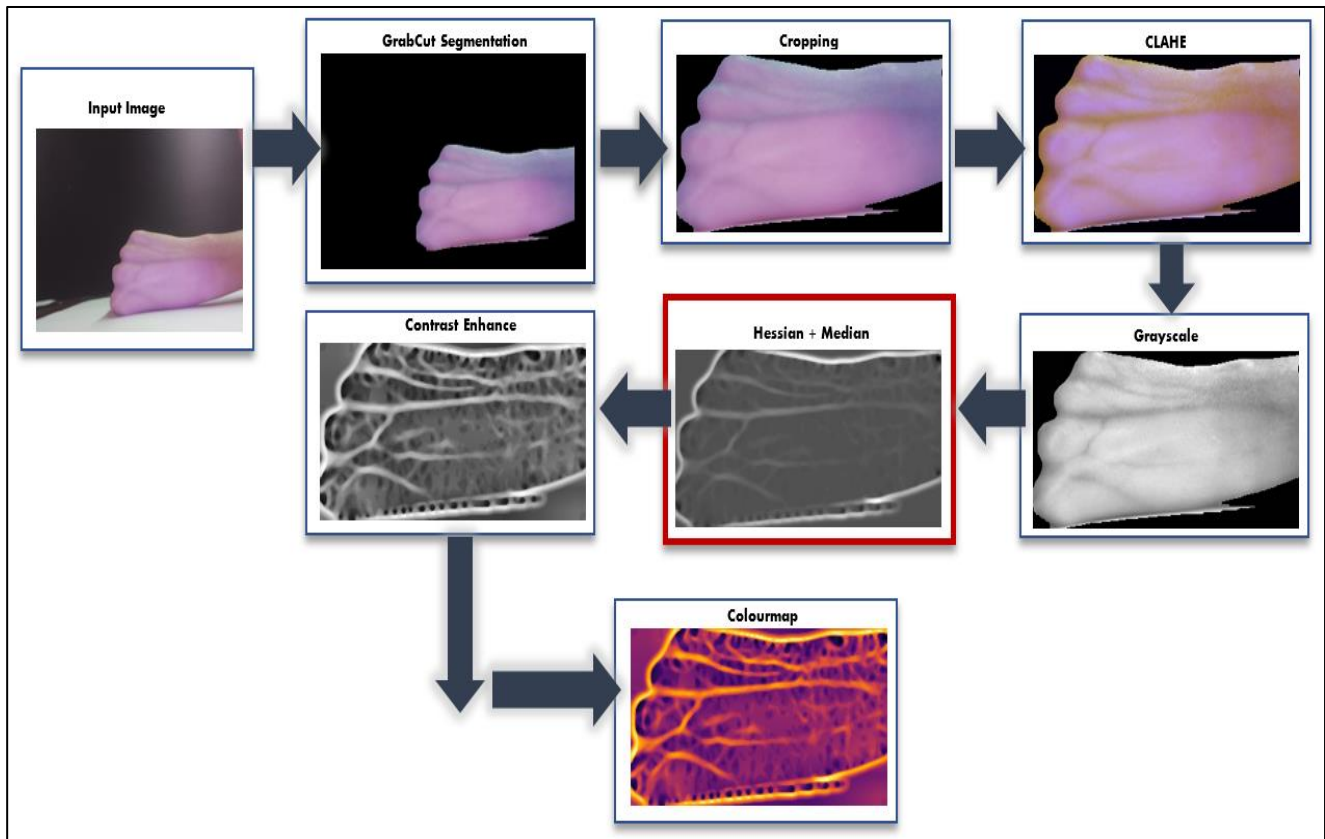


**Figure 7.** The overall image processing and morphological enhancement.

### 2.3.1. GrabCut Segmentation for ROI and Cropping

The GrabCut Segmentation process used iterative graph-based algorithms to disassociate the vein image's background and foreground. The method was designed to resemble a visible ROI. In this study, the GrabCut algorithm [17] using the Gaussian Mixture Models (GMMs) Color Clustering algorithm [18] were used to accomplish segmentation of a selected ROI and concurrently crop the selected ROI. Both strategies were extensively investigated [19]. The following algorithm showed the implementation of the proposed solutions.

To improve the process, the additional padding that emerges after the segmentation in the initial phase was cropped, leaving just the selected ROI in focus. The procedure for basic image cropping is included in the following algorithm.

### 2.3.2. CLAHE

Several strategies were put in the processing line to amplify the ridge's features on the vein image, starting by adopting the contrast-limited adaptive histogram equalization (CLAHE). The CLAHE method was used for better extraction of vessels as suggested by [4]. Adapting the adaptive histogram equalization (AHE) without improvement would lead to unnecessary over-amplified noise in relatively homogeneous regions of a vein image. Therefore, the best alternative was to limit the image contrast to a single color channel as suggested by CLAHE itself. The Algorithm 1 was the applied to implement CLAHE in this study.

**Algorithm 1** CLAHE

---

```

IN:   Image X of size  $M \times N$ 
OUT:  Contrast-enhanced image Y of the same size of image X
1     Segment the image into a number of non-overlapping tiles where each region is of size
       $8 \times 8$  (OpenCV default)
2     Compute the histogram of each segmented tiles
3     Let top = B = clipping limit
4     Let bottom = 0
5     FOR each segmented tile
6     Let S = sum of histogram bins of the excess in that bin over middle
7     WHILE  $top - bottom > 1$ 
8      $middle = (top + bottom) / 2$ 
9     IF  $S > (B - middle) * R$ 
10    top = middle
11    ELSE bottom = middle

```

---

## 2.3.3. Grayscale Conversion

Mordvintsev and Abid (2017) stated that the conversion from RGB color space to grayscale can be applied using the formula below:

$$\text{RGB[A]} \text{ to Gray: } Y \leftarrow 0.299 \cdot R + 0.587 \cdot G + 0.114 \cdot B$$

## 2.3.4. Hessian and Median Filter

Hessian segmentation uses eigenvalues to calculate the probability of the pixel being a vessel. According to Salima and Herdiyeni (2015), the quantitative estimation of the Hessian,  $\mathbf{H}$ , at each pixel of the given image,  $I(x, y)$ , is obtained.

$$\mathbf{H} = \begin{bmatrix} L_{xx} & L_{xy} \\ L_{yx} & L_{yy} \end{bmatrix} = \begin{bmatrix} \frac{\partial^2 I}{\partial x^2} & \frac{\partial^2 I}{\partial x \partial y} \\ \frac{\partial^2 I}{\partial y \partial x} & \frac{\partial^2 I}{\partial y^2} \end{bmatrix} \quad (1)$$

The entries of  $\mathbf{H}$  can be obtained at multiple scales by convolving the image  $I(x, y)$  with the two-dimensional Gaussian kernel  $G(x, y; \sigma)$  of different scales  $\sigma$ , which is defined as:

$$G(x, y; \sigma) = \frac{1}{2\pi\sigma^2} \exp^{-\frac{x^2+y^2}{2\sigma^2}} \quad (2)$$

where

$\pi = 3.142 \dots$

$\sigma$  = standard deviation for Gaussian Operation

$x$  and  $y$  = relative coordinate of the center of kernel

$$H_{xx} = \frac{\partial^2 I}{\partial x^2} = I(x, y) \times \sigma^2 G_{xx} \quad (3)$$

$$H_{xy} = H_{yx} = \frac{\partial^2 I}{\partial xy} = \frac{\partial^2 I}{\partial yx} = I(x, y) \times \sigma^2 G_{xy} \quad (4)$$

$$H_{yy} = \frac{\partial^2 I}{\partial y^2} = I(x, y) \times \sigma^2 G_{yy} \quad (5)$$

The eigenvalues can be determined by using the formula below:

$$\lambda_1 = \frac{L_{xx} + L_{yy} - \alpha}{2} \quad (6)$$

$$\lambda_2 = \frac{L_{xx} + L_{yy} + \alpha}{2} \quad (7)$$

where the local maxima,  $\alpha$ , are obtained using the formula below:

$$\alpha = \frac{\sqrt{(H_{xx} + H_{yy})^2 + 4(H_{xy})^2}}{2} \quad (8)$$

$H_{xx}$  = Second derivative in  $x$  – axis of the hessian matrix

$H_{yy}$  = Second derivative in  $y$  – axis of the hessian matrix

$H_{xy}$  = Second derivative in  $xy$  direction of the hessian matrix

To better understand the process, Algorithm 2 has been used to apply the Hessian matrix to an image.

---

**Algorithm 2** Hessian Matrix

---

IN: Grayscale image  $X$  of size  $M \times N$   
 OUT: Hessian-applied grayscale image  $Y$  of the same size of Image  $X$

- 1 Convolve the image using Gaussian Kernel in the order of  $H_{xx}$ ,  $H_{yy}$  and  $H_{xy}$
- 2 FOR every pixel in the image
- 3 Compute the covariance matrix
- 4 Calculate the local maxima and minima of the image using the eigenvalues from the covariance matrix:
- 5 Local Maxima =  $(H_{xx} + H_{yy})/2 + \text{sqrt}(4 * H_{xy} ** 2 + (H_{xx} - H_{yy}) ** 2)/2$
- 6 Local Minima =  $(H_{xx} + H_{yy})/2 - \text{sqrt}(4 * H_{xy} ** 2 + (H_{xx} - H_{yy}) ** 2)/2$

---

Median filtering is carried out in such a way that, a window is relocated from one column to the next along the rows of the image and the pixel's median enclosed within the window at every position is computed. The median of the individual pixel is calculated by taking neighboring pixels based on window size and then sorting them in ascending or descending order. Then, the middle value is considered the median, and the original pixel values are substituted with the median value. The mathematical annotation can be defined as:

$$y_{ij} = \text{med}(\{x_{uv} | x_{uv} \in N_{ij}\}) \quad (9)$$

Hessian and Median Filter approaches came next in the processing line to produce overlay ridges features on the vein image while reducing unnecessary noise along the process. Then, the image's contrast was again increased to make the shadows darker and highlights brighter. The last process that lies in the row was to enhance the overall quality of the vein image. This involved the color mapping procedure which maps the inferno features on the targeted vein image.

### 2.3.5. Contrast Enhance

Since the Hessian algorithm generated a low-contrast image, an increment of contrast is needed. This time, the clipping limit was 10. The clipping limit is determined by averaging the median and mean intensity values. This was to make the vein more apparent and distinct as the higher the clipping limit, the higher the contrast of the image. However, if the clipping limit is too high, the probability that the feature becomes obscure is high.

### 2.3.6. Colormap

Color mapping is a function that maps one image's colors to a different image's colors. A color mapping may be referred to as the algorithm that results in the mapping function or the algorithm transforming the colors of the image. In this project, the color map inferno was used. Inferno is a perceptually uniform color map with monotonically increasing luminance. It is like a black body but also adds some purple hues for a more appealing display. Inferno is one of the matplotlib color maps developed by Stéfan van der Walt and Nathaniel Smith [20]. The following algorithm demonstrates the process of applying a colormap on an image.

### 2.4. Data Evaluation: Vein Counting

There are three veins visible in the antecubital fossa. The median cubital vein should be the primary option among the three veins in the middle of the arm, followed by the veins in the lateral aspect (outer thumb side), which is the cephalic vein, and the veins in the medial aspect (inner little finger side), which is the basilic vein [21]. The median cubital vein is thought to be the ideal location for venepuncture. It is described as firmly anchored, big and noticeable [22], and acts as a branching between the two major veins [23]. These were the veins detected during prototype testing, with special attention on the median cubital vein [24].

The number of veins apparent in both palm and arm was counted by visual examination after image enhancement. The number of vein counts was recorded and compared. A branching vein, having a Y-shape as in Figure 8, was counted as consisting of two [25]. If there was uncertainty about whether the ROI was indeed a vein or a shadow, it was not included in the count. Rules for counting were consistent for both palm and arm.

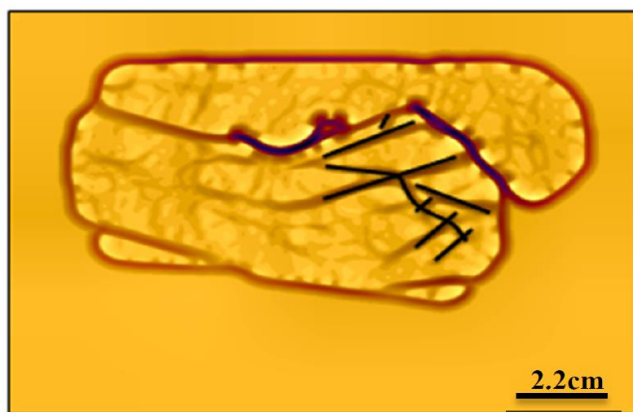


Figure 8. Vein counting applied (black line) on the image named CP85M9.

## 3. Results and Discussion

The findings of this study are divided into three parts:

1. Evaluation analysis of near-infrared LEDs wavelength and arrangement.
2. Evaluation analysis of selected wavelength with diffuser in a square LED arrangement.
3. Evaluation analysis of square LED arrangement for vein visualization.

### 3.1. Evaluation of Near Infrared LEDs Wavelength and Arrangement

Images captured at different incident wavelengths were processed to evaluate the performance of each LEDs wavelength. The vein was captured as a black line on the picture when exposed to near-infrared radiation [26]. The haemoglobin absorbs the NIR radiation, which causes it to appear darker than other tissues [26].

The image status was denoted as fail (X) and pass (O). Table 4 shows the findings for both arm and palm using either square LED or ring LED arrangement of the NIR light at wavelengths ranging from 720 nm to 940 nm. Fail (X) indicates that the vein images failed to be acquired, and vice versa.

Table 4. Status for arm and palm with wavelength range from 720 nm to 940 nm.

(λ)	Arm (Square) (9 LEDs)	Arm (Ring) (8 LEDs)	Palm (Square) (9 LEDs)	Palm (Ring) (8 LEDs)
720 nm	X	X	X	X
760 nm	X	X	X	O
850 nm	O	O	O	O
900 nm	O	O	O	O
940 nm	O	O	O	O

The first evaluation focused on the LEDs wavelength, comparing the 720 nm, 760 nm, 850 nm, 900 nm, and 940 nm. Furthermore, each wavelength image was acquired using ring LED and square LED of the LEDs light arrangement. Figures 9 and 10 only show the successfully acquired vein images at ROI of palm and arm areas. The 720 nm wavelength was unable to visualize the vein because the wavelength's penetration depth falls between visible light and near-infrared radiation. The optical penetration of human skin is found to be deepest at wavelengths approaching 1090 nm when tested light penetration for wavelengths ranging from 400 nm to 2000 nm [5]. The light penetration depth in human tissue is mostly affected by the absorption and scattering of light radiation. Moreover, the beam angle of the LEDs limits the area of illumination, as can be seen in Figure 9 (images with labels HP72M9 and HP72R8).

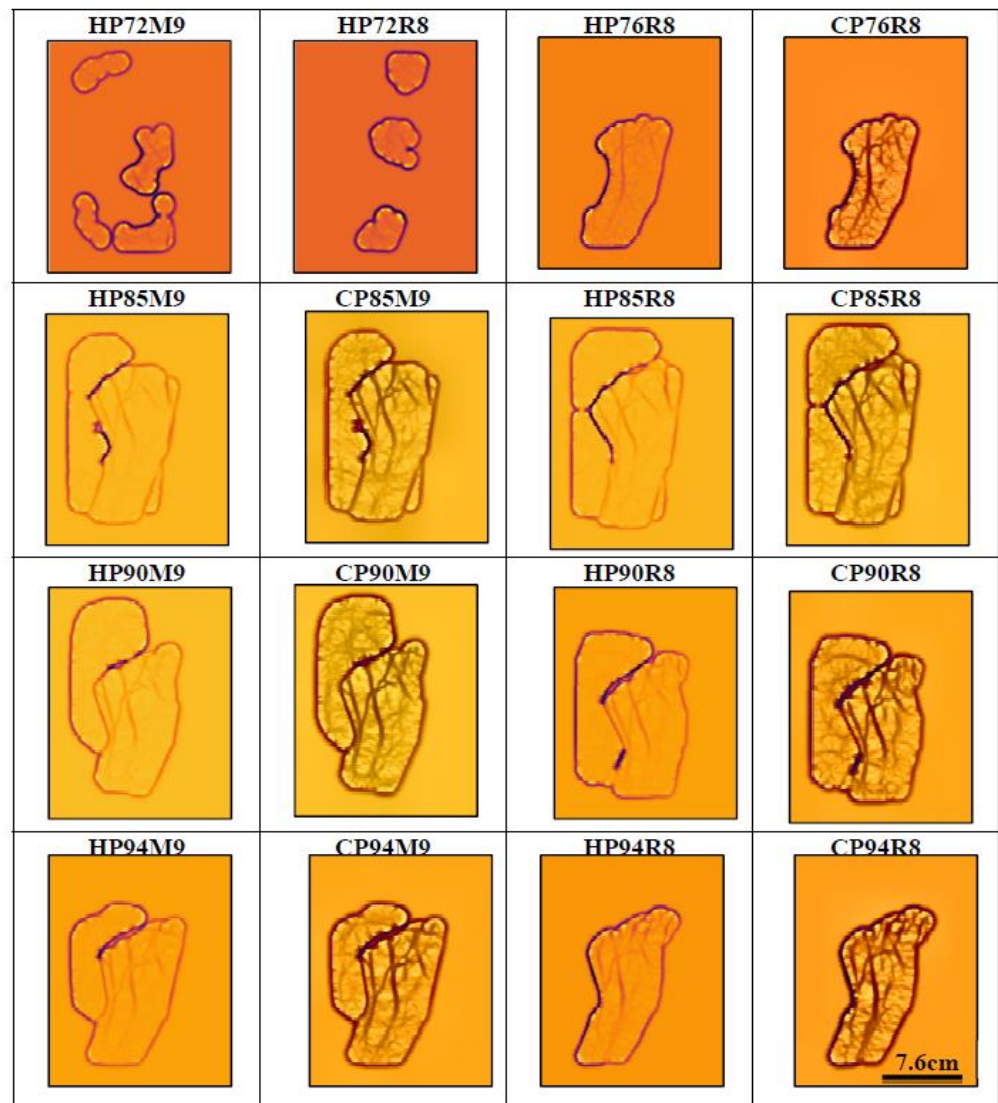


Figure 9. Images for palm area.

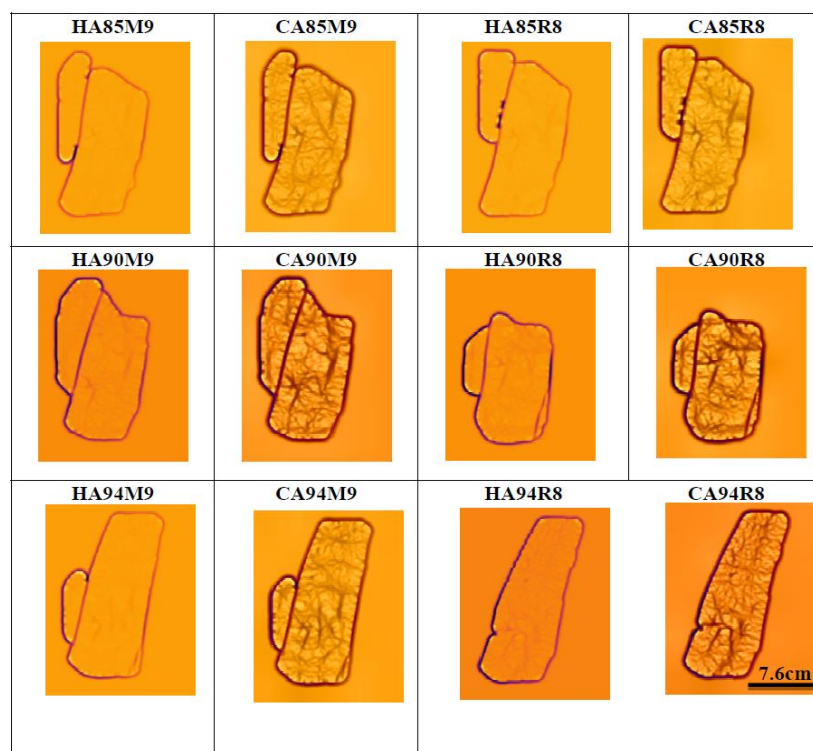


Figure 10. Images for arm area.

The square LED and ring LED arrangement of LEDs modified the radiation intensity distribution. The images in Figures 9 and 10 compared the entire wavelengths in the palm area for square LED and ring LED. Figures 9 and 10 show that the square LED illuminates both palm and arm areas better based on the physical visualization of the images obtained. The image labeled CA90M9 square LED-based has better visualization compared with the image labeled CA90R8.

Table 5 shows that an incident wavelength of 850 nm yields the highest number of veins counts with images labeled CA85M9 and CA85R8. Isolated and big vessels were found, especially in the palm area. The peak wavelength of 850 nm has good scattering light propagation characteristics in human tissue, hence providing a better penetration effect [13]. However, little and tortuous structures were better found with wavelengths between 850 and 900 nm. The 900 nm wavelength light created more shadow, which made another line be detected as a vein. The result of 940 nm and 900 nm was similar in terms of vein counts, except the shadow was more obvious at a wavelength of 900 nm. The ring LED arrangement vein counts were higher than the square LED arrangement for the palm area, which was caused by the additional vein counts of the infrared wavelength 760 nm images.

Table 5. Vein counting on palm and arm areas at different incident wavelengths.

(λ)	HPM9	CPM9	HPR8	CPR8	HAM9	CAM9	HAR8	CAR8
720 nm	1	1	1	1	0	0	0	0
760 nm	0	0	3	3	0	0	0	0
850 nm	7	8	7	8	3	3	3	3
900 nm	7	8	7	8	3	3	2	2
940 nm	7	8	6	5	3	3	1	1

The average thickness of the epidermis is 0.2 mm; however, this thickness varies based on the location of the body and the volume of water that the epidermis retains. The dermis is the second layer of skin located underneath the epidermis. This layer is significantly thicker than the epidermis (often 1 to 4 mm) [27]. This sublayer has fewer nerve fibers

and capillaries than the papillary layer and has a denser and thicker network. In many early investigations on skin optics, the epidermis and the dermis are treated as separate optical mediums. Since the epidermis lacks veins and capillaries, haemoglobin can only be found in the dermis. The third layer below the dermis is subcutaneous tissue. It is crucial to remember that it is not considered an additional skin layer. The average thickness of this layer is stated to be 4 to 9 mm [28].

NIR radiation enables the sight of veins 3–5 mm beneath the skin, commonly employed for catheterization or blood draws [14]. In the upper arm, the average thickness of the skin is 2.00 mm (2.14 mm in men and 1.84 mm in females) [29]. The epidermis of the human palm is the thickest (approximately 1.5 mm) [23]. The dermis (thin inner skin) contains fewer blood vessels than the arm [23]. In terms of NIR light penetration, the arm skin layer has a thicker dermis layer that is an excellent site for vein imaging.

Figure 11 reveals that the total vein counting applying the HR (Hessian Ring LED) image processing technique for the palm area was higher than the HM (Hessian Square LED) arrangement as the number of vein counts on the image 760 nm was included. Furthermore, the image processing encounters an error to process the 760 nm images for the square LED arrangement, causing it to be omitted as the selected wavelength. The studied area produced the same findings for the contrast method, either square LED or ring LED arrangement on the palm. Figure 12 reveals that both HM (Hessian Square LED) and CM (Contrast Square LED) showed the same number of vein counts on the arm area.

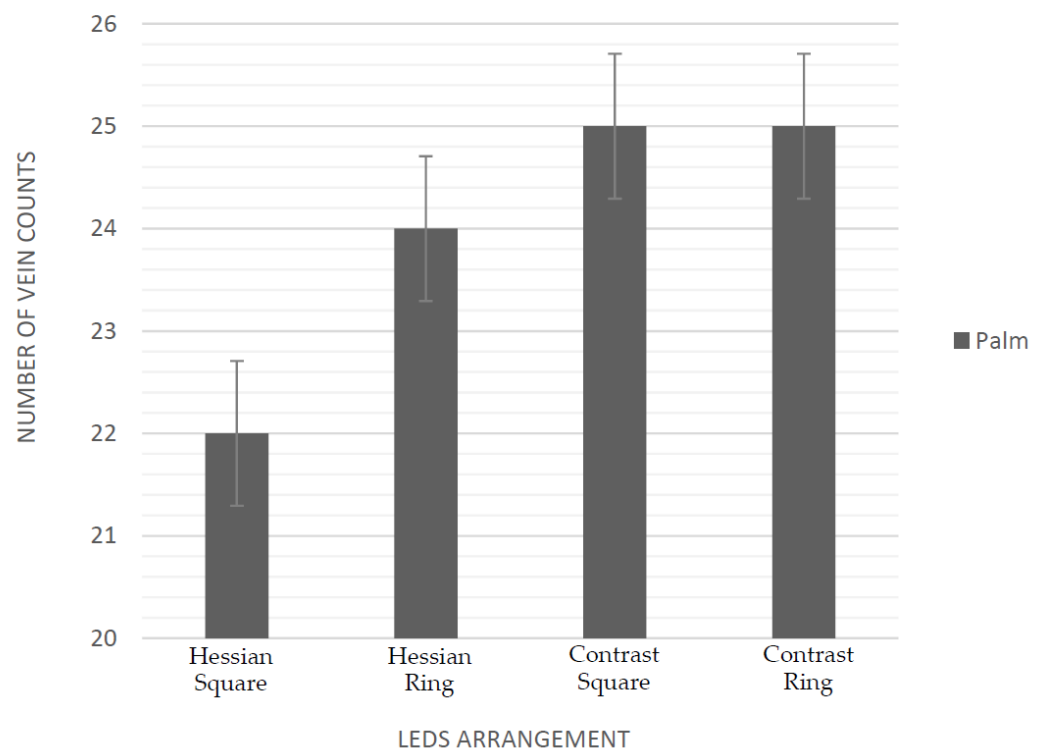


**Figure 11.** Number of vein counts vs LEDs arrangement for the palm area.

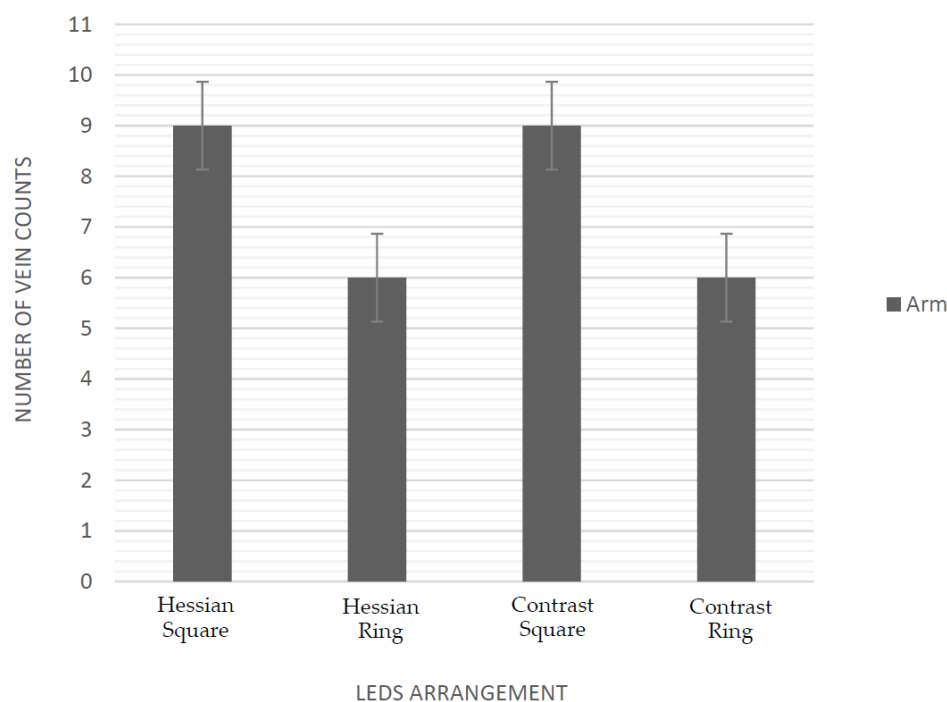


**Figure 12.** Number of vein counts vs LEDs arrangement for arm area.

Near-infrared radiation is able to penetrate human tissue [1]. Infrared radiation was focused on the palm and arm area for this current study. An increase in the penetration depth can be achieved using longer wavelengths of light [30]. However, the composition in blood vessels, such as water, oxyhaemoglobin and deoxyhaemoglobin affected the penetration and absorption processes in the vein. This is because epidermal energy absorption depends on the water content [31]. Furthermore, human skin absorbs light differentially where the absorption can be increased by the deoxygenated blood haemoglobin [32]. For the 850 nm wavelength, the composition of water is lower compared to the composition of deoxyhaemoglobin and oxyhaemoglobin. Therefore, it has a low affinity to water, causing the wavelength to be absorbed more by the vein.

In terms of the LEDs arrangements, the ring LED arrangement creates a non-uniform light distribution and the center area of the region of interest was not illuminated enough. The result in the arm area shows the same result, whereas the square LED arrangement has shown a more promising result. The increase in the square LED is considered sufficiently significant, even if the number of vein counting is increased by one. Hence, the counting was focused on the arm area since it is commonly used for venepuncture. Different configurations are studied for the simplicity and accuracy of the illumination process. These configurations include ring LED and square LED arrangements for the light radiation source. While both of the presented arrangement configurations offer a good contrast in the region of interest, the results from the experiments suggested that the square LED arrangement LEDs provide better results in terms of radiation distribution and uniformity [33].

The radiation distribution at the region of interest after being irradiated with an NIR light also depends on the features of the LEDs. The optical power emitted by the LEDs and irradiation time for this experiment in both ring LED and square LED arrangements is set to be the same. If the optical powers of the light are not the same, it will manipulate the effectiveness of penetration depth [13]. However, in this evaluation, all of the features are controlled.

### 3.2. Evaluation Analysis of Selected Wavelength with Diffuser Using Square LED Arrangement

In this experiment, the selected wavelength is 850 nm, and the square LED arrangement was used as it has a better area of illumination based on the findings in Section 1. After the image processing for both methods was performed as shown in Figure 13, the

shape of the vein in both arm and palm appears as a Type II human vein arrangement [34], where the NIR light was filtered with diffuser paper HA85M16W and CA85M16W. Overall, the addition of a diffuser was found not to be one of the crucial parameters for enhancing the vein visualization system.

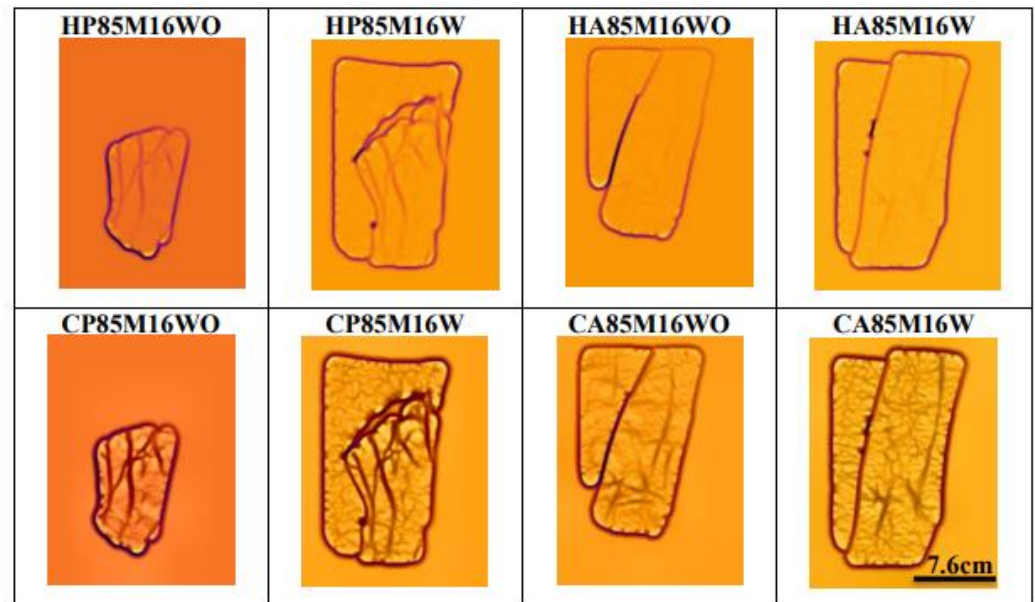


**Figure 13.** Images for palm (P) and arm (A) area with addition of diffuser.

Our findings showed that the number of vein counts for both ROIs was similar with or without the diffuser. The only drawback of the absence of a diffuser is the lack of uniformity of the light source [33]. This can be easily fixed by adding layers of diffusers in front of the LEDs to achieve more constant illumination. The diffuser scatters the light from the LEDs, diminishing the radiation intensity. This study proved that a diffuser paper could attenuate the IR source so that the radiation can be distributed more uniformly [27] even though there is no significant difference in the results.

### 3.3. Evaluation of Square LED Arrangement for the Light Illuminator

In this experiment, the square LED arrangement was used as justified by the findings in Section 1. Square LED arrangement provides more constant illumination that covers the ROI. Images with different square LED arrangements were processed to compare the performance of each arrangement. For the  $5 \times 5$  and  $6 \times 6$  arrangements, the light illumination intensity was too bright, producing only black and white images. However, the processed images for  $6 \times 6$  arrangements as shown in Figure 14 resemble the human vein arrangement based on Yamada et al., 2008 and reveal a clearer image of veins than other square LED arrangements.

Figure 15 shows that the number of vein counts for HM3X3, CM3X3, HM5X5 and CM5X5 are the same. Figure 15 strongly reveals that a  $6 \times 6$  square LED arrangement provides the best outcome for the arm area.

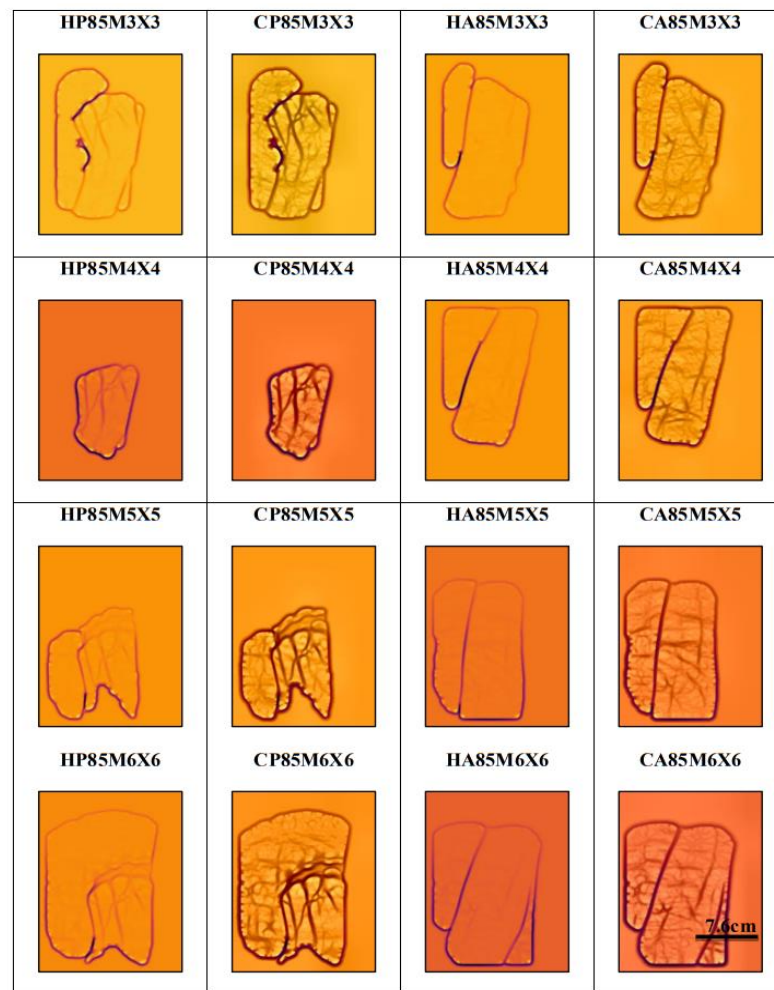


Figure 14. Images for palm and arm area for square LED arrangement.

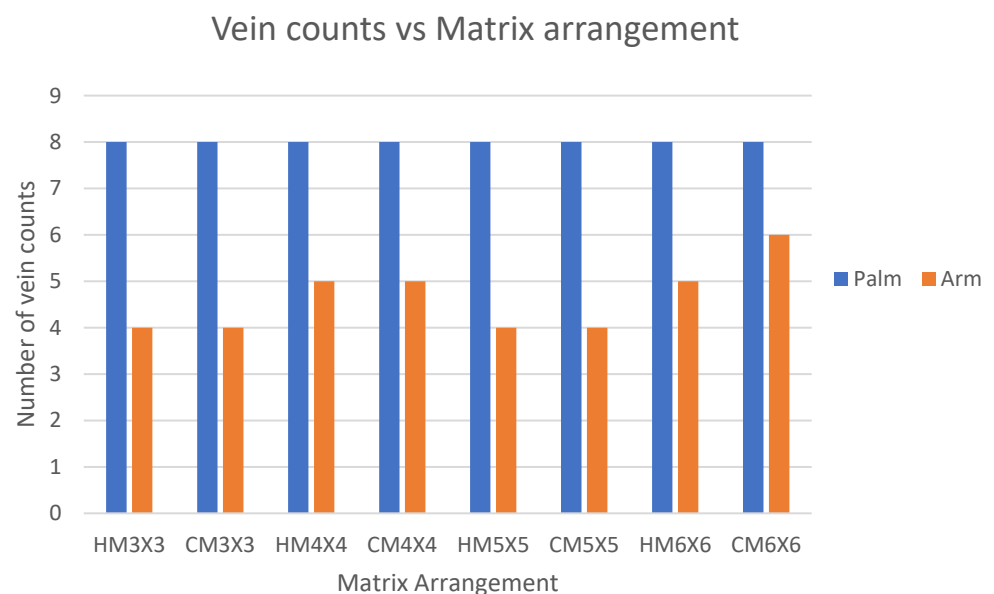


Figure 15. Hessian method for square LED arrangement.

The use of multiple LEDs would result in an overlapping illumination pattern. Experiments have shown that various square LED arrangements of the LEDs will alter the

radiation intensity distribution. This is mainly because the system uses an absorption method, and the camera must be placed on the same side as the light source. In this experiment, the increase in square LED arrangement not only increases the illumination area but also enlarges the shadow from the light source. This study reveals that increasing the square LED arrangement of the NIR is not to be perceived as one of the significant design parameters in the vein visualization process. This statement can be supported by the observation of difficulty in the penetration of light towards the arm area due to the thicker epidermis of the skin. Furthermore, thicker skin can cause the wavelength to degrade its energy as it passes through a deeper layer of the skin.

#### 4. Conclusions

This research focused on analyzing four design parameters to improve the design of the vein visualization system: the evaluation of NIR wavelength, the LEDs arrangement for light illumination purposes, the effect of the diffuser and the number of LEDs. Light illumination with a wavelength of 850 nm is found to provide a better vein visualization due to its excellent light scattering characteristics in human tissue. This study also shows that the square LED arrangement of LEDs as a light source provides excellent uniformity of light radiation.

In this research, the light diffuser was not considered one of the key parameters for the light illumination process. Although the noise removal of the image makes the image processing performed faster, it does not contribute to improving the vein count. Increasing the square LED arrangement will increase the illumination area, but the vein's absorption did not show much improvement. Nevertheless, a physical response derived from a human's vein after being irradiated depends on the tissue's biological properties and the LED's features as a light source. The contrast method shows a more promising vein image enhancement than the Hessian method.

These evaluations are crucial for developing a novel vein visualizing system, particularly in vein image acquisition techniques that have not yet been investigated thoroughly in the literature. The solution suggested in this current research can help provide useful inputs on developing imaging devices for medical procedures.

**Author Contributions:** Investigation, A.B.A.R. and F.J.; Supervision, F.P.C. and A.B.; Validation, F.K. All authors have read and agreed to the published version of the manuscript.

**Funding:** This research was funded by Universiti Malaysia Sabah with project no. SDN0018-2019 and GUG0318-2019.

**Institutional Review Board Statement:** Not applicable.

**Informed Consent Statement:** Not applicable.

**Acknowledgments:** The authors of this paper would like to thank Universiti Malaysia Sabah for supporting this research by providing research grants.

**Conflicts of Interest:** The authors declare no conflict of interest.

#### References

1. Cuper, N.J.; Verdaasdonk, R.M.; De Roode, R.; De Vooght, K.M.K.; Viergever, M.A.; Kalkman, C.J.; De Graaff, J.C. Visualizing Veins with Near-Infrared Light to Facilitate Blood Withdrawal in Children. *Clin. Pediatr.* **2011**, *50*, 508–512. [[CrossRef](#)] [[PubMed](#)]
2. Fuksis, R.; Greitans, M.; Nikisins, O.; Pudzs, M. Infrared Imaging System for Analysis of Blood Vessel Structure. *Elektron. Ir Elektrotechnika* **2010**, *97*, 45–48.
3. Kim, D.; Kim, Y.; Yoon, S.; Lee, D. Preliminary Study for Designing a Novel Vein-Visualizing Device. *Sensors* **2017**, *17*, 304. [[CrossRef](#)] [[PubMed](#)]
4. Azueto-Ríos, Á.; Hernández-Gómez, L.-E.; Hernández-Santiago, K.-A. Forearm and Hand Vein Detection System for an Infrared Image Database. *Res. Comput. Sci.* **2016**, *127*, 137–147. [[CrossRef](#)]
5. Yaprak, E.; Kayaalti-Yukse, S. Preliminary Evaluation of Near-Infrared Vein Visualization Technology in the Screening of Palatal Blood Vessels. *Med. Oral Patol. Oral Cir. Bucal* **2018**, *23*, e98–e104. [[CrossRef](#)]
6. Wang, L.; Leedham, G. Near- and Far- Infrared Imaging for Vein Pattern Biometrics. In Proceedings of the IEEE International Conference on Video and Signal Based Surveillance 2006, AVSS 2006, Sydney, NSW, Australia, 22–24 November 2006.

7. Qadir, Z.; Direkoğlu, C. European Journal of Engineering and Applied Sciences Time and Cost-Efficient Vein Pattern Recognition and Injection Point Suggestion Using Machine Vision Technology. *App. Sci.* **2019**, *2*, 58–64.
8. Alwazzan, M.J. Low Cost Blood Vein Detection System Based on Near-Infrared LEDs and Image-Processing Techniques. *Polish J. Med. Phys. Eng.* **2020**, *26*, 61–67. [[CrossRef](#)]
9. VT, G. A Novel Design Proposal for Low-Cost Vein-Viewer for Medical and Non-Contact Biometric Applications Using NIR Imaging. *J. Med. Eng. Technol.* **2021**, *45*, 303–312. [[CrossRef](#)] [[PubMed](#)]
10. Chowdhury, T.; Khan, S.; Faruk, T.; Islam, M.K. Design and Implementation of a Low-Cost Real-Time Vein Imaging for Developing Countries. In Proceedings of the 2021 International Conference on Automation, Control and Mechatronics for Industry 4.0, ACMI 2021, Rajshahi, Bangladesh, 8–9 July 2021. [[CrossRef](#)]
11. Liu, X.; Chen, H.; Montieri, A.; Pescapè, A. Human Behavior Sensing: Challenges and Approaches. *J. Ambient Intell. Humaniz. Comput.* **2020**, *11*, 6043–6058. [[CrossRef](#)]
12. Swarbrick, J.; Boylan, C.J. *Encyclopedia of Pharmaceutical Technology: Volume 19—Blood Substitutes: Hemoglobin-Based Oxygen Carriers to Tablet Evaluation Using Near-Infrared Spectroscopy*; Informa Health Care: London, UK, 1999.
13. Madrid García, A.; Horche, P.R. Light Source Optimizing in a Biphotonic Vein Finder Device: Experimental and Theoretical Analysis. *Results Phys.* **2018**, *11*, 975–983. [[CrossRef](#)]
14. Juhim, F.; Chee, F.P.; Rahman, A.B.A.; Bade, A. Effect of Exposure Time of Near Infrared Light Radiation (NIR) on Human's Vein Visualization. *Int. J. Recent Technol. Eng.* **2020**, *8*, 2072–2075. [[CrossRef](#)]
15. Nundy, K.K.; Sanyal, S. A Low Cost Vein Detection System Using Integrable Mobile Camera Devices. In Proceedings of the Proceedings of the 2010 Annual IEEE India Conference: Green Energy, Computing and Communication, INDICON 2010, Kolkata, India, 17–19 December 2010.
16. Crisan, S.; Tebrean, B. Low Cost, High Quality Vein Pattern Recognition Device with Liveness Detection. Workflow and Implementations. *Meas. J. Int. Meas. Confed.* **2017**, *108*, 207–216. [[CrossRef](#)]
17. Rother, C.; Kolmogorov, V.; Blake, A. "GrabCut". In Proceedings of the ACM SIGGRAPH 2004 Papers on—SIGGRAPH'04; ACM Press: New York, NY, USA, 2004; p. 309.
18. Orchard, M.T.; Bouman, C.A. Color Quantization of Images. *IEEE Trans. Signal Process.* **1991**, *39*, 2677–2690. [[CrossRef](#)]
19. Mordvintsev, A.; Abid, K. OpenCV-Python Tutorials Documentation. 2017. Available online: [https://opencv24-python-tutorials.readthedocs.io/\\_/downloads/en/stable/pdf/](https://opencv24-python-tutorials.readthedocs.io/_/downloads/en/stable/pdf/) (accessed on 16 June 2022).
20. Moreland, K. Colour Map Advice for Scientific Visualization. Available online: <https://www.kennethmoreland.com/color-advice> (accessed on 20 April 2019).
21. CLSI. *Collection of Diagnostic Venous Blood Specimens—Seventh Edition. GP41*; CLSI: Wayne, PA, USA, 2017; Volume 37, p. 84.
22. Ogden-Grable, H.; Gill, G.W. Phlebotomy puncture juncture: Preventing phlebotomy errors—Potential for harming your patients. *Lab. Med.* **2005**, *36*, 430–433. [[CrossRef](#)]
23. Buowari, O.Y. Complications of Venepuncture. *Adv. Biosci. Biotechnol.* **2013**, *4*, 126–128. [[CrossRef](#)]
24. Pan, C.-T.; Francisco, M.D.; Yen, C.-K.; Wang, S.-Y.; Shiu, Y.-L. Vein Pattern Locating Technology for Cannulation: A Review of the Low-Cost Vein Finder Prototypes. *Sensors* **2019**, *19*, 3573. [[CrossRef](#)]
25. Mela, C.A.; Lemmer, D.P.; Bao, F.S.; Papay, F.; Hicks, T.; Liu, Y. Real-Time Dual-Modal Vein Imaging System. *Int. J. Comput. Assist. Radiol. Surg.* **2019**, *14*, 203–213. [[CrossRef](#)]
26. Chandra, F.; Wahyudianto, A.; Yasin, M. Design of Vein Finder with Multi Tuning Wavelength Using RGB LED. *J. Phys. Conf. Ser.* **2017**, *853*. [[CrossRef](#)]
27. Ong Michael, G.K.; Connie, T.; Jin Teoh, A.B. A Contactless Biometric System Using Palm Print and Palm Vein Features. In *Advanced Biometric Technologies*; InTech: Rijeka, Croatia, 2011.
28. Hwang, H.; Yim, J.; Cho, J.; Cheon, C.; Kwon, Y. 110 GHz Broadband Measurement of Permittivity on Human Epidermis Using 1 Mm Coaxial Probe. In Proceedings of the IEEE MTT-S International Microwave Symposium Digest, Philadelphia, PA, USA, 8–13 June 2003; Volume 1, pp. 399–402.
29. Juric, S.; Flis, V.; Debevc, M.; Holzinger, A.; Zalik, B. Towards a Low-Cost Mobile Subcutaneous Vein Detection Solution Using Near-Infrared Spectroscopy. *Sci. World J.* **2014**, *2014*, 365902. [[CrossRef](#)]
30. Ash, C.; Dubec, M.; Donne, K.; Bashford, T. Effect of Wavelength and Beam Width on Penetration in Light-Tissue Interaction Using Computational Methods. *Lasers Med. Sci.* **2017**, *32*, 1909–1918. [[CrossRef](#)]
31. Farkas, J.P.; Hoopman, J.E.; Kenkel, J.M. Five Parameters You Must Understand to Master Control of Your Laser/Light-Based Devices. *Aesthetic Surg. J.* **2013**, *33*, 1059–1064. [[CrossRef](#)] [[PubMed](#)]
32. Ahmed, K.I.; Habaebi, M.H.; Islam, M.R. A Real Time Vein Detection System. *Indones. J. Electr. Eng. Comput. Sci.* **2018**, *10*, 129. [[CrossRef](#)]
33. Crisan, S.; Tarnovan, I.G.; Crisan, T.E. Radiation Optimization and Image Processing Algorithms in the Identification of Hand Vein Patterns. *Comput. Stand. Interfaces* **2010**, *32*, 130–140. [[CrossRef](#)]
34. Yamada, K.; Yamada, K.; Katsuda, I.; Hida, T. Cubital Fossa Venipuncture Sites Based on Anatomical Variations and Relationships of Cutaneous Veins and Nerves. *Clin. Anat.* **2008**, *21*, 307–313. [[CrossRef](#)] [[PubMed](#)]